Cell Reports
Article

Arabidopsis Accelerated Cell Death 11, ACD11, Is a Ceramide-1-Phosphate Transfer Protein and Intermediary Regulator of Phytoceramide Levels

Dhirendra K. Simanshu,[1,8] Xiuhong Zhai,[2,8] David Munch,[3] Daniel Hofius,[3,9] Jonathan E. Markham,[4] Jacek Bielawski,[5] Alicja Bielawska,[5] Lucy Malinina,[6] Julian G. Molotkovsky,[7] John W. Mundy,[3,*] Dinshaw J. Patel,[1,*] and Rhoderick E. Brown[2,*]

[1]Structural Biology Program, Memorial Sloan-Kettering Cancer Center, New York, NY 10065, USA
[2]Hormel Institute, University of Minnesota, Austin, MN 55912, USA
[3]Department of Biology, BioCenter, University of Copenhagen, 2200 Copenhagen N, Denmark
[4]Department of Biochemistry, University of Nebraska, N146 Beadle Center, Lincoln, NE 68588, USA
[5]Department of Biochemistry and Molecular Biology, Lipidomics Shared Resource Mass Spectrometry Lab, Medical University of South Carolina, Charleston, SC 29425, USA
[6]Structural Biology Unit, CIC bioGUNE, Technology Park of Bizkaia, 48160 Derio-Bilbao, Spain
[7]Shemyakin-Ovchinnikov Institute of Bioorganic Chemistry, Russian Academy of Sciences, 117997 Moscow, Russia
[8]These authors contributed equally to this work
[9]Present address: Department of Plant Biology and Forest Genetics, Swedish University of Agricultural Sciences and Linnean Center for Plant Biology, Uppsala BioCenter, 75007 Uppsala, Sweden
*Correspondence: mundy@science.ku.dk (J.W.M.), pateld@mskcc.org (D.J.P.), reb@umn.edu (R.E.B.)
http://dx.doi.org/10.1016/j.celrep.2013.12.023

SUMMARY

The *accelerated cell death 11* (*acd11*) mutant of *Arabidopsis* provides a genetic model for studying immune response activation and localized cellular suicide that halt pathogen spread during infection in plants. Here, we elucidate ACD11 structure and function and show that *acd11* disruption dramatically alters the in vivo balance of sphingolipid mediators that regulate eukaryotic-programmed cell death. In *acd11* mutants, normally low ceramide-1-phosphate (C1P) levels become elevated, but the relatively abundant cell death inducer phytoceramide rises acutely. ACD11 exhibits selective intermembrane transfer of C1P and phyto-C1P. Crystal structures establish C1P binding via a surface-localized, phosphate headgroup recognition center connected to an interior hydrophobic pocket that adaptively ensheaths lipid chains via a cleft-like gating mechanism. Point mutation mapping confirms functional involvement of binding site residues. A π helix (π bulge) near the lipid binding cleft distinguishes apo-ACD11 from other GLTP folds. The global two-layer, α-helically dominated, "sandwich" topology displaying C1P-selective binding identifies ACD11 as the plant prototype of a GLTP fold subfamily.

INTRODUCTION

Sphingolipids and their metabolites (i.e., ceramide [Cer], ceramide-1-phosphate [C1P], and the long-chain bases [LCBs] sphingosine and sphingosine-1-phosphate [S1P]), are bioactive lipids that function as messenger signals and mediators of eukaryotic processes such as cell growth, development, embryogenesis, senescence, inflammation, and programmed cell death (PCD) (Fyrst and Saba, 2010; Hannun and Obeid, 2008; Michaelson and Napier, 2010). The dynamic balance between Cer (sphingoid base amide linked to a fatty acyl chain) and its phosphorylated derivative, C1P, critically regulates PCD in plants and animals (Berkey et al., 2012; Chen et al., 2009; Pata et al., 2010; Reape and McCabe, 2008).

In plants, PCD occurs during development, during disease symptoms associated with virulent infections, and during the hypersensitive response (HR) induced by avirulent stress effectors (Lam, 2004). Hallmarks of HR are local accumulation of reactive oxygen species, nitric oxide, and the phytohormone, salicylic acid (SA). By inducing localized cell death triggered when resistance proteins recognize specific pathogen-derived molecules, HR potentiates defensive resistance. Mutants exhibiting *accelerated cell death* (*acd*) phenotypes in the absence of pathogen effectors also provide insights into HR-like PCD and defense activation. One HR mimic is the *acd5* mutant, which lacks Cer kinase (CerK) activity and accumulates Cers, triggering PCD (Liang et al., 2003). C1P addition partially abrogates the PCD-inducing effects of elevated Cer in *acd5*. In *acd11* null mutant, HR-related PCD and defense genes are constitutively

activated in a SA-dependent fashion. The *acd11* gene encodes ACD11, a lipid transfer protein able to moderately accelerate the intermembrane transfer of sphingosine and sphingomyelin (SM), but not Cer or glycosylceramides (Brodersen et al., 2002; Petersen et al., 2008).

Structural homology modeling predicts that ACD11 forms a GLTP fold and is a glycolipid transfer protein (GLTP) superfamily member (Airenne et al., 2006; Brown and Mattjus, 2007; Petersen et al., 2008). Yet, ACD11 is unable to transfer glycolipids (Brodersen et al., 2002), consistent with the lack of essential residues needed for glycosphingolipid (GSL) sugar headgroup binding (Petersen et al., 2008). In mammalian GLTPs and HET-C2 fungal GLTP, X-ray structures reveal the molecular details of how glycolipids are recognized and bound by a conserved residue cluster (Asp, Asn, Lys, His, and Trp) that forms a hydrogen bond network with the GSL sugar-amide region, thus explaining the selectivity and transfer proficiency for various GSLs (Airenne et al., 2006; Kenoth et al., 2010, 2011; Malinina et al., 2004, 2006; Samygina et al., 2011). Currently lacking for ACD11 is the establishment of its preferred sphingolipid ligand as well as direct evidence for its functional involvement in the regulation of plant sphingolipid metabolism.

Herein, we investigated ACD11 structure and lipid transfer specificity and discovered high selectivity for C1P and phyto-C1P, but not related plant sphingolipids, i.e., glucosylceramides (GlcCers), Cer, glycosylinositolphosphoceramides (GIPCs), and sphingoid LCBs. X-ray structures establish ACD11 global architecture to be a GLTP fold and reveal the molecular basis for selective recognition of C1P. Point mutation functional analyses support structural mapping showing a cationic residue cluster mediating the selective binding of the C1P headgroup in a surface-located recognition cavity. An intrahelical distortion, i.e., π helix (π bulge), uniquely distinguishes ACD11 from other known GLTP folds including the recently discovered human ceramide-1-phosphate transfer protein (CPTP) (Simanshu et al., 2013). The π bulge involves key residues of the C1P recognition center that regulates access and encapsulation of the lipid hydrocarbon chains to an adjoining hydrophobic pocket. In *Arabidopsis acd11* (*acd11-1*) null mutant, normally low C1P levels are elevated, whereas relatively abundant phytoceramides (phyto-Cers) rise acutely, consistent with shifts in the dynamic balance and distributions of these two sphingolipids playing a key role in plant PCD regulation.

RESULTS

ACD11 Forms a GLTP Fold with a Helical π Bulge in Its Lipid Headgroup Recognition Center

To experimentally establish if ACD11 forms a GLTP fold, we crystallized wild-type (WT) protein and determined its structure (1.8 Å) (Tables S1 and S2). ACD11 adopts the two-layer, all α-helical "sandwich" motif characteristic of the GLTP fold (Figure 1A). Nonetheless, there are differences compared to the human GLTP fold prototype (Figure S1). At the N terminus, ACD11 has an extra α helix (designated αN) that is lacking in human GLTP and is ~35% shorter in human CPTP. Key residues involved in lipid headgroup recognition in ACD11 (Figure 1B, cyan) differ in GLTP (Figure 1B, pink), but not in CPTP (Figure 1C, beige), except for conserved Asp60 and His143, residues needed for Cer interaction in all GLTP folds (Figure S1A, red). The ACD11 C-terminal region does not directly contribute to formation of the headgroup recognition cavity as occurs in GLTP (Figure 1B, red arrow) but resembles the HET-C2 fungal GLTP fold, which terminates similarly with a Trp residue (Kenoth et al., 2010). In ACD11, C-terminal Trp206 positioning is stabilized by cation-pi interaction with Arg92, but no similar interaction occurs in GLTP or CPTP, which end with Val209 and Pro214, respectively. A relatively small, compact cavity for lipid headgroup binding exists in ACD11 and CPTP, a consequence of the α3/α4 loop projecting out and over in hood-like fashion (Figure 1B, blue arrow; Figure 1C). The nearby surface region is highly basic (Figures 1D and 1F) compared to its more neutral counterpart in human GLTP (Figure 1E). A noteworthy structural feature of apo-ACD11 is the π helix (π bulge) in helix α2 near Asp60 resulting in close proximity to His143 via a 2.9 Å salt bridge (Figures 1G and 1J). In all other known apo-GLTP folds including CPTP, no π bulge occurs, and the analogous Asp and His residues remain further apart (Figures 1H and 1I).

Crystal Structure of ACD11 in Complex with Lysosphingomyelin

The first tests of ACD11 transfer of GSL and related metabolites (Brodersen et al., 2002) preceded crystal structure determination of the human GLTP fold and mapping of the glycolipid binding site (Malinina et al., 2004). GLTP and ACD11 superpositioning (Figure 1B) reveals a positively charged residue triad (K64, R99, and R103) in ACD11 replacing N52, L92, and W96 in GLTP. This explains the lack of glycolipid transfer by ACD11 and limited transfer of SM, which has a phosphocholine headgroup (Petersen et al., 2008). Thus, initial trials focused on cocrystallization of WT-ACD11 complexed with SM and lysosphingomyelin (lysoSM) (Figure 2A). Only the latter lipid yielded a crystal complex enabling 2.4 Å resolution (Figures 2B–2D; Table S1). The expected lipid-headgroup recognition cavity is occupied by a sulfate ion from crystallization solution. Also adsorbed nearby on the protein surface is the sphingoid chain of lysoSM. Notably, the choline headgroup moiety projects outward and away from the protein surface (Figures 2B–2D). One phosphate oxygen undergoes hydrogen bonding with the amide nitrogen of Gly144, whereas the sphingoid base amine hydrogen bonds with Asp60 (Figure 2D). The π bulge centered at Asp60 (α2 helix) persists in the ACD11/lysoSM complex. At the crystal-packing interface of the asymmetric unit, an additional lysoSM molecule is observed (Figure S2A).

ACD11 Is a C1PTP

Because plants contain no SM and do not produce this sphingolipid, SM transfer by ACD11 was surprising, suggesting that SM serves as a substitute analog for the plant lipid preferred in vivo (Petersen et al., 2008). Also, as noted earlier, the lipid headgroup binding cavity is relatively small, compact, and hood-like (Figure 1B, blue arrow), an arrangement expected to poorly accommodate the bulky SM phosphocholine headgroup. With that in mind, WT-ACD11 was analyzed for intermembrane transfer of other sphingolipids and phosphoglycerides. A Förster resonance energy transfer approach involving probe lipids with

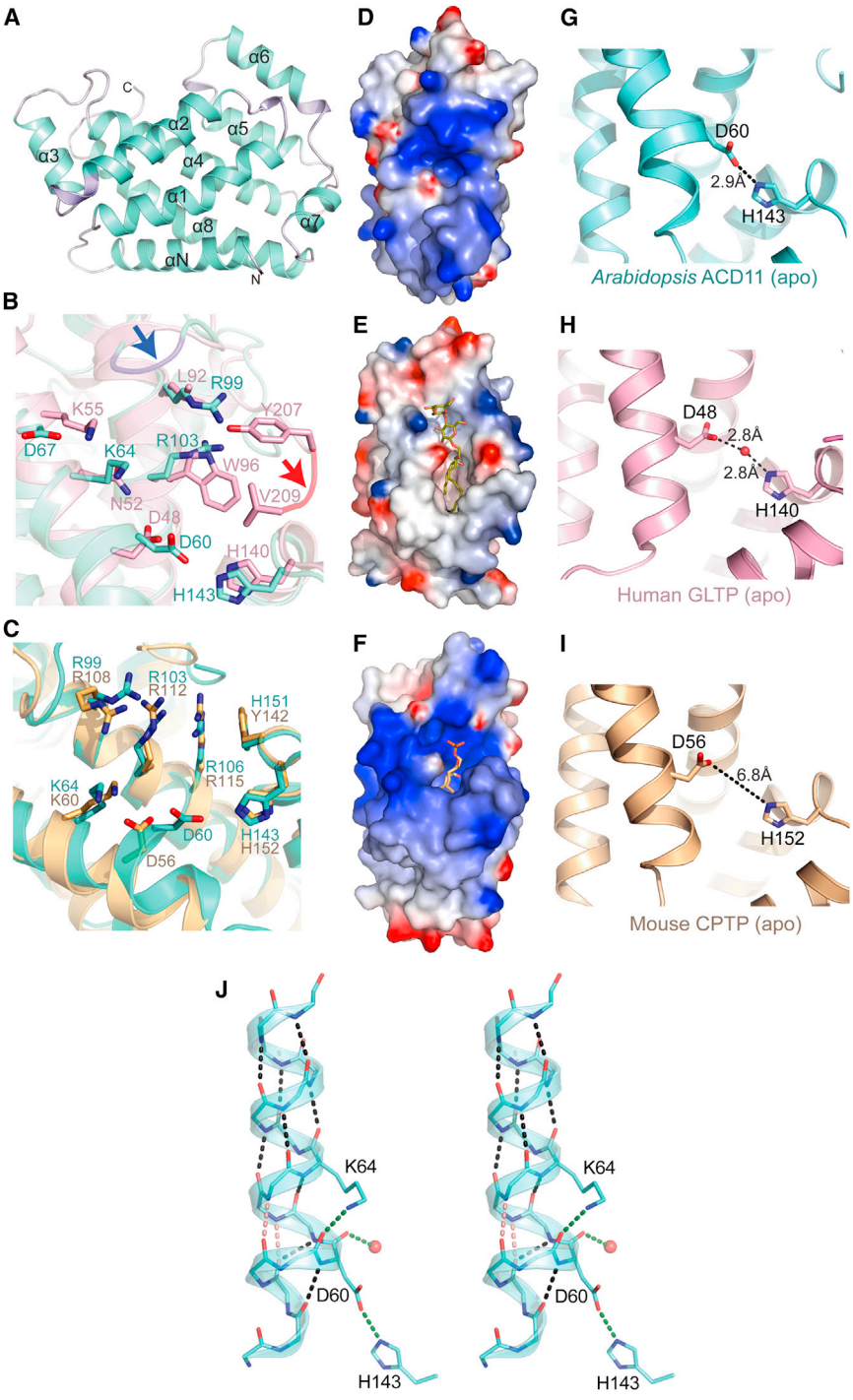

Figure 1. Crystal Structure of *Arabidopsis* ACD11, Comparison with Human GLTP and CPTP Structures, and π Bulge in ACD11 Lipid Headgroup Binding Pocket

(A) GLTP fold of apo-ACD11 (ribbon) showing arrangement of α helices (cyan) and 3_{10} helices (lavender).

(B) Structural superposition of ACD11 (cyan) and human GLTP (pink) comparing side chains (stick representation) involved in lipid headgroup recognition. Blue and red arrows show insertion loop in ACD11 (lavender highlights) and human GLTP (red highlights), respectively, near the lipid headgroup binding pocket.

(C) Structural superposition of ACD11 (cyan) and mouse CPTP (tan) comparing side chains (stick representation) involved in phosphate headgroup recognition.

(D) ACD11 surface electrostatics showing positively charged region around the lipid headgroup binding cavity. Blue indicates positive charge.

(E) Surface electrostatics of human GLTP bound to 18:1 LacCer (stick representation) showing larger, neutral (white) cavity for binding lipid sugar headgroup.

(F) Surface electrostatics of human CPTP bound to C1P (stick representation).

(G) π bulge centered on Asp60 promotes salt bridge formation between Asp60 (α2 helix) and His143 (α5/α6 loop).

(H) In human apo-GLTP, there is no π bulge centered on Asp48, and interaction with His140 occurs via water bridging.

(I) In mouse CPTP, there is no π bulge centered on Asp56 and no water-mediating interaction with His152.

(J) Stereo view of π bulge in ACD11 α2 helix. Hydrogen bond types *i*→*i-4* and *i*→*i-5* are shown as black and pink dashed lines, respectively. Interactions among Asp60 and neighboring His143, Lys64, and a water molecule are shown as green dashed lines.

See also Figures S1 and S7 and Tables S1, S2, and S3.

acyl-linked anthrylvinyl (AV) fluorophore enabled testing of lipids with phosphate headgroups, i.e., AV-phosphatidic acid (AV-PA) and AV-C1P, and controls, i.e., AV-galactosylceramide (AV-GalCer), AV-SM, and AV-Cer. ACD11 robustly transferred AV-C1P (sphingoid based), but not AV-PA (glycerol based) (Figures 2E and 2F). Notably, ACD11 also transferred AV-phyto-C1P (Figures 2E and 2F), as expected by modeling of phyto-C1P docking in the ACD11 binding site. The sphingoid chains of "phyto" sphingolipid derivatives that predominate in plants lack the 4,5 *trans* double bond but contain a 4-hydroxy group (Markham et al., 2006, 2013). The AV-C1P and AV-phyto-C1P transfer rates depended on protein concentration, required acceptor membranes (Figures 3B, S3A, and S3B), and proceeded at ~4.5 C1P and ~5.6 phyto-C1P molecules/min/protein. Replacement of phosphate with sugar (AV-GalCer) prevented transfer by ACD11, but not by GLTP. AV-SM transfer by ACD11 was very slow (Figure 2E). The lack of AV-Cer transfer suggested a requirement for phosphate in the headgroup for functionality. This was confirmed by competition against AV-C1P transfer by lipids containing natural hydrocarbon chains (Figure 2G). Only nonfluorescent C1P

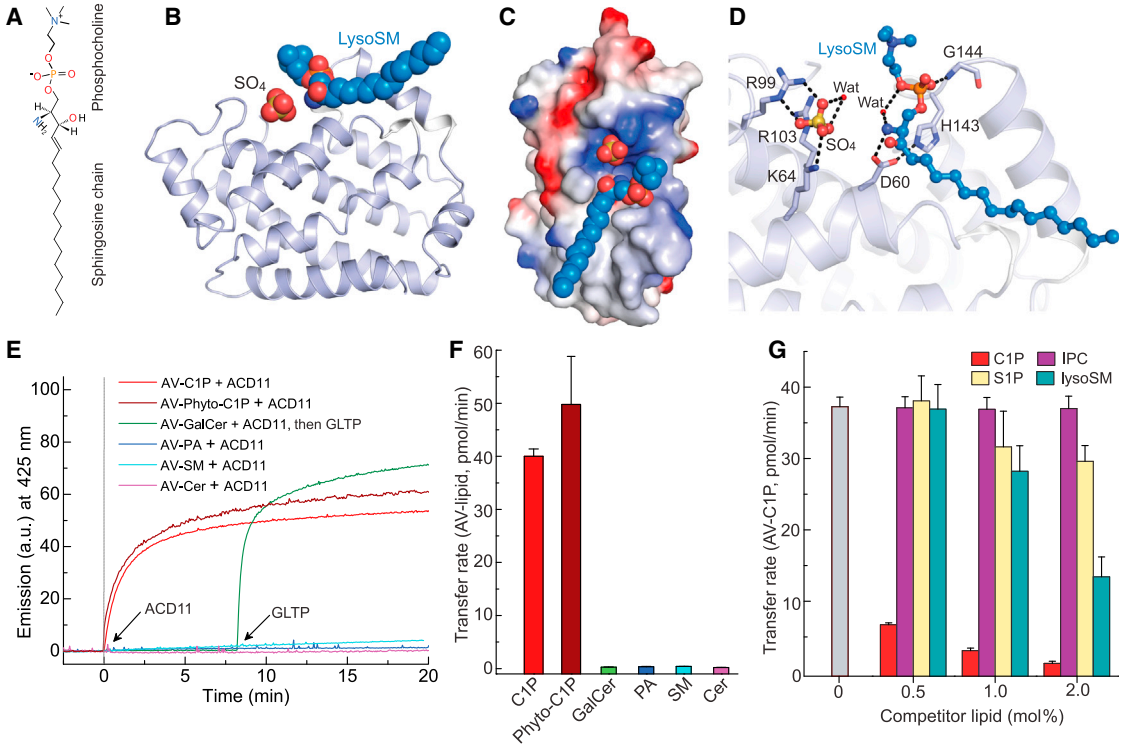

Figure 2. Crystal Structure of ACD11 in Complex with lysoSM and ACD11 Lipid Transfer Specificity

(A) Structure of lysoSM.

(B) Crystal structure of ACD11/lysoSM complex showing ACD11 (ribbon) bound to lysoSM and sulfate (space filling).

(C) Surface electrostatics of ACD11 in complex with lysoSM.

(D) Lipid headgroup recognition center residues (lavender) interacting with lysoSM (blue, ball-and-stick) and sulfate. Dashed lines show hydrogen bonds.

(E) Lipid transfer in vitro by Förster resonance energy transfer.

(F) Quantification of initial lipid transfer rates in (E).

(G) Competition against AV-C1P transfer by nonfluorescent lipids. 18:1-C1P competes strongly, lysoSM moderately, S1P weakly, and IPC nearly nil (see Figures S3C–S3F for kinetic traces).

See also Figures S2 and S3 and Tables S1 and S3.

competed strongly against AV-C1P (Figure S3C). IPC (inositol-phosphoceramide), S1P, lysoSM, and N-hexyl(6:0)-SM (data not shown) exerted differing weak competition (Figures 2G and S3D–S3F). PA and lysoPA minimally slowed the initial AV-C1P transfer rate and were not effective competitors (Figure S3G).

Crystal Structure of D60N/D60A-ACD11 with Bound C1P

Due to the high transfer specificity for C1P, extensive cocrystallization trials were initiated for WT-ACD11 and C1P, but no positive outcome ensued. To achieve success, a point mutation strategy was used to weaken the Asp60-His143 salt bridge associated with the π bulge. We focused on Asp60 because mutation of the analogous Asp (D48V) in human GLTP is reasonably well tolerated (Samygina et al., 2011). Asp60 was mutated to residues expected to weaken (Asn) or eliminate (Ala) salt bridging with H143. The D60N-ACD11 mutant maintained ~25%–30% activity, whereas D60A-ACD11 was ~10%–15% active compared to WT-ACD11 (Figure 3B).

Both the D60N and D60A mutants yielded crystal complexes with N-dodecanoyl-C1P (12:0-C1P) (Figure 3; Tables S1 and S3), but not with other lipids (e.g., S1P, sphingosine, SM, lysoSM, or PA). In the D60N-ACD11/12:0-C1P crystal complex, the asymmetric unit consists of two ACD11 molecules containing 12:0-C1P bound in two ways (Figures 3C–3F). In one case, both the sphingosine and lauroyl acyl chain of 12:0-C1P are encapsulated in the hydrophobic pocket (Figures 3C and 3E). In the other case, only the lauroyl acyl chain is inserted into the hydrophobic pocket, whereas the sphingosine chain remains outside the pocket (Figures 3D and 3F). With D60A-ACD11/12:0-C1P complex, a different crystal form was observed involving one protein molecule with bound 12:0-C1P (Figure 3G; Tables S1 and S3). However, the overall structure resembled the sphingosine-out binding mode displayed by D60N-ACD11/12:0-C1P complex (Figures 3G and 3H). Similar sphingosine-out conformers have been observed in human GLTP complexed with GSLs (Malinina et al., 2006; Samygina et al., 2011, 2013) and in human CPTP complexed with C1P (Simanshu et al., 2013). Similar positioning of different C1P species occurs in the hydrophobic pockets of ACD11 and CPTP except for the obvious differences in the bending angle of the outwardly projecting sphingoid chain in the sphingosine-out binding mode (Figure S4).

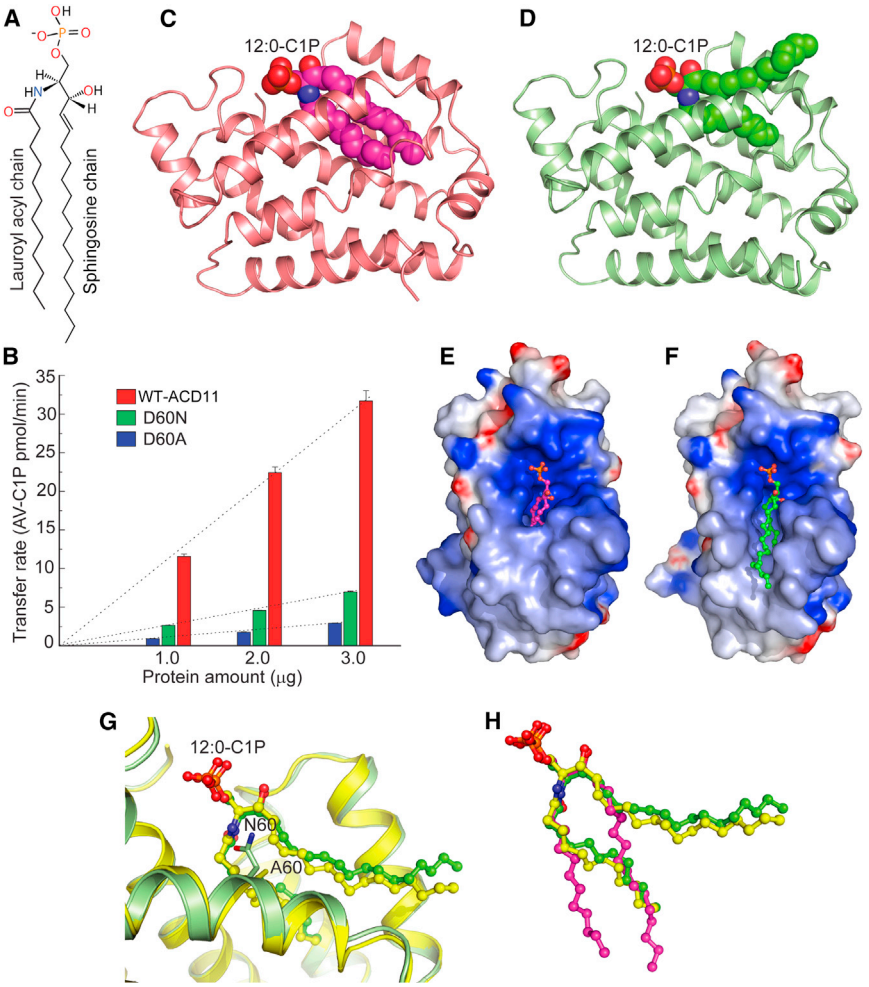

Figure 3. Crystal Structures of D60N/D60A-ACD11 in Complex with 12:0-C1P and Their C1P Transfer Activities

(A) Structure of 12:0-C1P.

(B) C1P initial transfer rates by WT-ACD11 (red), D60N-ACD11 (green), and D60A-ACD11 (blue) using 3 μg each.

(C) D60N-ACD11 (ribbon) in complex with 12:0-C1P showing the acyl and sphingosine chains both buried in the hydrophobic pocket (sphingosine-in mode; space filling) in one molecule of the crystal asymmetric unit.

(D) D60N-ACD11 (ribbon) in complex with 12:0-C1P (space filling) with the acyl chain buried in the hydrophobic pocket and the sphingosine chain adsorbing to the protein surface (sphingosine-out mode) in the second molecule of the crystal asymmetric unit.

(E) Surface electrostatics of D60N-ACD11 with bound 12:0-C1P (sphingosine-in mode; ball-and-stick).

(F) Surface electrostatics of D60N-ACD11 with bound 12:0-C1P (sphingosine-out mode).

(G) Structural superposition of C1P headgroup binding pocket of D60N-ACD11 (green) and D60A-ACD11 (yellow) in complex with 12:0-C1P showing the disappearance of π bulge in α2 helix.

(H) Structural comparison of 12:0-C1P binding to D60N-ACD11 (sphingosine-in, magenta and sphingosine-out, green) and to D60A-ACD11 (sphingosine-out, yellow).

See also Figures S4 and S7 and Tables S1 and S3.

The bending of sphingosine occurs immediately distal to the 4,5 *trans* double bond where carbon-carbon single bonds exist and torsional rotation is unrestrained, providing conformational optimization for packing at the crystal contact faces of ACD11 and CPTP.

Recognition of C1P by ACD11

It is noteworthy that the π bulge in apo-ACD11 (helix α2) disappears upon binding of C1P in both D60N- and D60A-ACD11, presumably reflecting C1P-induced conformational changes related to portal opening and entry of one or both C1P hydrocarbon chains into the hydrophobic pocket (Figures 3G, 4A, and 4B). In both 12:0-C1P conformer complexes with D60N- and D60A-ACD11, the C1P group is anchored to positively charged residues on the protein surface via interaction of the three phosphate oxygen atoms with Lys64, Arg99, and Arg103 (Figure 4C). Their functional importance is illustrated by severe reductions in C1P transfer for the K64A, R99E, R99A, and R103A point mutants (Figure 4F). The C1P amide moiety hydrogen bonds with His143 and Asn60. The net effect is disruption of the stabilizing salt bridge and elimination of the π bulge characteristic of apo-ACD11.

The hydrophobic pocket that accommodates the sphingosine and acyl chains of C1P is formed by a cluster of nonpolar residues, i.e., Leu, Val, Ile, Phe, Met, Ala, and Tyr, that line the two layers of the α helices in ACD11 (Figure 4D). Insertion and encapsulation of the 12:0-C1P hydrocarbon chains result in the disappearance of the intrahelical π bulge. This π helix-to-α helix structural transition involves large conformational changes for the side chains of several residues, i.e., Phe47, Phe54, Phe56, and Leu50 (Figure 4E), which move toward the protein surface. This effectively expands the hydrophobic pocket and creates space to accommodate the hydrocarbon chains of 12:0-C1P. Introduction of polarity into the hydrophobic pocket by point mutation (F47Q-ACD11) leads to diminished activity (Figure 4F), affirming the importance of the hydrophobic environment. In the "sphingosine-out" structures, the nonpolar amino acids between helices α5 and α6 interact with the sphingoid chain via hydrophobic and van der Waals interactions enabling adsorption to the protein surface when encapsulation by the hydrophobic pocket does not occur.

Crystal Structure of D60A-ACD11 in Complex with N-Acetyl-C1P

To define C1P features that contribute to the π helix-to-α helix transition needed for C1P chain insertion into the hydrophobic pocket, D60A-ACD11 was cocrystallized with bound

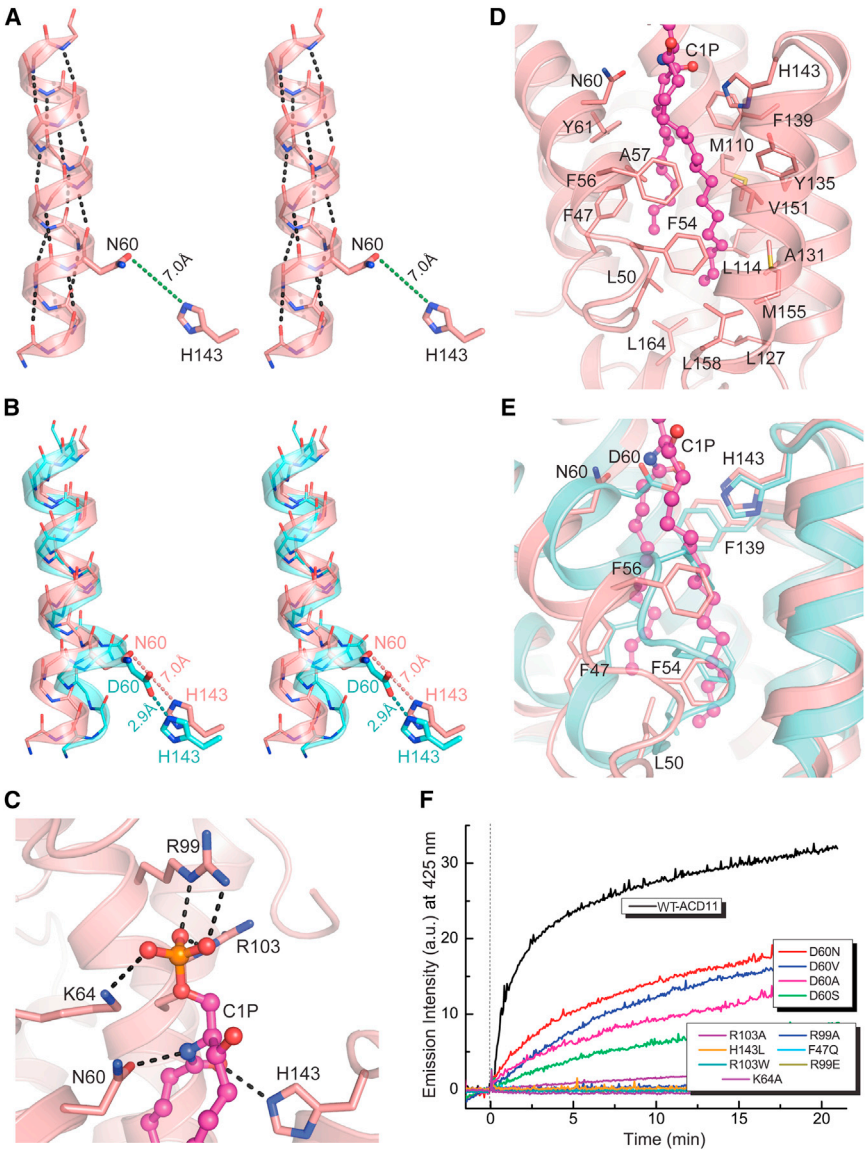

Figure 4. π Helix Transition to α Helix Induced by C1P Binding in D60N-ACD11 and Mapping of C1P Binding Site

(A) Stereo representation of α2 helix in the D60N-ACD11/12:0-C1P crystal complex showing absence of π bulge.

(B) Stereo view of structural superposition of α2 helix observed in apo-ACD11 (cyan) forming a π bulge and in D60N-ACD11 (salmon) in complex with 12:0-C1P structure without a π bulge. For clarity, only side-chain atoms of Asp60 and His143 are shown.

(C) 12:0-C1P and amide interactions with D60N-ACD11 residues in the headgroup binding cavity. Hydrogen bonds are shown by dashed lines.

(D) ACD11 residues forming the hydrophobic pocket that accommodates the C1P acyl and sphingosine chains.

(E) Localized conformational changes in apo-ACD11 and D60N-ACD11. Structural superposition of apo-ACD11 and D60N-ACD11/12:0-C1P complex shows residues undergoing large conformational changes during accommodation of C1P hydrocarbon chains. Bound C1P atoms (ball-and-stick) are colored magenta, red, and blue for carbon, oxygen, and nitrogen, respectively. apo-ACD11 and D60N-ACD11 side chains are colored cyan and salmon, respectively.

(F) C1P intervesicular transfer by ACD11 point mutants measured using Förster resonance energy transfer.

N-acetyl(2:0)-C1P (Figures 5A–5E; Tables S1 and S3). As expected, the phosphate headgroup hydrogen bonds with Lys64, Arg99, and Arg103, but the bidentate hydrogen bonding of Arg99 observed with 12:0-C1P (Figure 4C) is reduced to a single hydrogen bond (Figure 5C). The acetyl chain amide group is unable to hydrogen bond with Ala60 and fails to hydrogen bond with His143 (Figure 5C), leaving the acetyl group on the surface, turned away from Ala60 and outside the hydrophobic pocket. The sphingosine chain also remains outside the hydrophobic pocket (Figures 5B and 5E), adsorbed between helices α5 and α6 on the protein surface. In this altered "binding state," the π bulge persists, suggesting that transitioning of π helix to α helix is enhanced when the C1P acyl chain is long enough to enter the hydrophobic pocket (Figure 5D). From the functional standpoint, N-acetyl-C1P competes poorly against AV-C1P transfer by ACD11 (Figure 5F), as also is the case for S1P (Figure 2G). By contrast, N-acetyl-C1P competes moderately well against CPTP-mediated AV-C1P transfer (Simanshu et al., 2013), and the structure of the CPTP/N-acetyl-C1P complex shows no missing hydrogen bond interactions with the C1P-amide region, proper engagement of the N-acetyl group in the binding cleft, and encapsulation of the sphingoid chain in the hydrophobic pocket. The differences in position and conformation of bound N-acetyl-C1P molecules in ACD11 and CPTP are shown in Figure S5.

Perturbations of Sphingolipid Levels in *acd11-1* Mutants

To elucidate whether ACD11 involvement in *Arabidopsis* PCD manifests itself by altering sphingolipid metabolism, sphingolipid levels were profiled in dying leaves of homozygous *acd11-1* mutants. An overall accumulation of total sphingolipids (Figure 6A) including LCBs (Figure S6A) is evident in *acd11* compared to the *Landsberg erecta* (*Ler*) WT background, with total free Cers showing the greatest elevation. In plants, the dominant Cer species (>90%) are phyto-Cers (Markham et al., 2006, 2013), which reportedly are more potent inducers of PCD than Cer (Hwang et al., 2001). To verify and differentiate between effects caused by spontaneous cell death and reduced growth in *acd11*, we monitored sphingolipid levels upon PCD

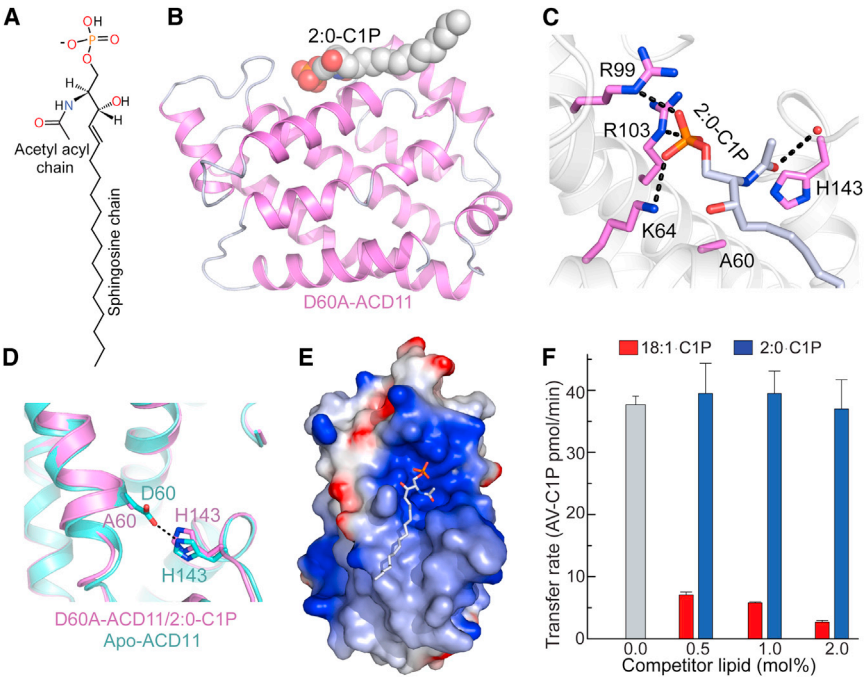

Figure 5. Crystal Structure of D60A-ACD11 in Complex with N-acetyl-C1P

(A) Structure of 2:0-C1P.

(B) Crystal structure of D60A-ACD11 (ribbon representation) in complex with 2:0-C1P (space filling) in sphingosine-out conformation.

(C) Inverted (flipped) orientation of lipid amide-acetyl group in sphingosine-out binding mode of 2:0-C1P complexed with D60A-ACD11.

(D) Enlarged view of α2 helix showing π bulge in the superposed structures of apo-ACD11 and D60A-ACD11 in complex with 2:0-C1P.

(E) Surface electrostatics of D60A-ACD11/2:0-C1P complex (stick representation).

(F) Competition against ACD11-mediated AV-C1P transfer by 2:0-C1P.

See also Figure S5 and Tables S1 and S3.

induction in *acd11*/NahG plants at 0, 12, 24, 72, and 120 hr after treatment with benzo(1,2,3)thia-diazole-7-carbothioic acid (BTH), a SA analog. Introduction of the bacterial transgene NahG into the *acd11* background removes endogenous SA needed for development of the cell death phenotype. When *acd11*/NahG plants are then treated with BTH, cell death is fully reinstated. By 72 and 120 hr after BTH treatment (Figure 6B), a large increase in total Cer is evident compared to *Ler* and NahG controls, as well as a minor rise in 2-hydroxyceramide, which may reflect free Cer hydroxylation or increased sphingolipid turnover. In contrast, levels of GlcCer and GIPC remain largely unaltered (Figure 6B), suggesting that their increase in *acd11* (Figure 6A) is probably due to reduced growth or the dwarf phenotype. Changes in levels of LCB(P), i.e., sphingoid-1-phosphates, also are insignificant in *acd11* (Figure S6B) and, thus, may take more time or require stronger inductive conditions (e.g., higher BTH/SA levels) to develop. C1P, which occurs at extremely low levels at normal growth temperature, was not detected. The observed perturbations of sphingolipid levels reveal Cer accumulation during development of *acd11* cell death, suggesting that ACD11 mediates Cer synthesis in a SA-dependent manner.

Because cold temperature treatment of *Arabidopsis* induces substantial and rapid elevation of C1P and LCB(P) by a transduction process regulated by endogenous nitric oxide (Cantrel et al., 2011), the responses of C1P and related sphingolipids to reduced temperature were analyzed in the *acd11* background. Figure 7A shows that *acd11* loss of function results in 3- to 5-fold elevations in the levels of different C1P species of plants subjected to cold treatment. These are quantitative determinations of C1P mass levels in plants, which were previously detected by radiolabeling (Cantrel et al., 2011). Also evident are moderate increases in LCBP, but not LCB (Figure 7B), and dramatic elevations of phyto-Cers (Figure 7C). Interestingly, with phyto-Cer, the palmitoyl (16:0) species and very long acyl species (22–26 carbons) are most affected, whereas the elevations with C1P are shifted to the moderately long acyl species (16–22 carbons). These changes are consistent with a complex regulatory mechanism involving ACD11.

DISCUSSION

Unique Structural Aspects of the Lipid Headgroup Recognition Center and Hydrophobic Pocket of the ACD11 GLTP Fold

Despite low sequence homology of ACD11 and other GLTP homologs including human CPTP (Figure S1A), our crystallographic data establish the conserved structural homology shared by *Arabidopsis* ACD11, human GLTP, and human CPTP (Simanshu et al., 2013) while revealing important differences. Unlike GLTP but like CPTP, ACD11 contains a modified lipid headgroup recognition center that selectively binds C1P, an important signaling lipid linked to cell survival. Comparison of ACD11, GLTP, and CPTP with their preferred bound lipids suggests adaptation and evolutionary conservation of key residues in their GLTP folds. The net outcome is two divergent subfamilies within the GLTP superfamily. Residues adapted to focus lipid specificity to C1P in ACD11 include Lys64 for Asn52, Arg99 for Leu92, and Arg103 for Trp96 in GLTP. The clustered Lys/Arg residues of ACD11 form a positively charged triad that is ideally arranged for binding phosphate, explaining the inability of ACD11 to bind sugar headgroups and transfer glycolipids (Petersen et al., 2008). It is noteworthy that Arg103 occupies the same position where Trp acts as a stacking plate for the Cer-linked headgroup sugar in human GLTP, fungal HET-C2, plant GLTP1, and human FAPP2 (Kamlekar et al., 2013; West et al., 2008). Conversely, residues analogous to Asp60 and His143 of ACD11 are absolutely conserved in the lipid headgroup recognition centers of all known GLTP folds. The "pincher-like" clamping that occurs when Asp and His hydrogen

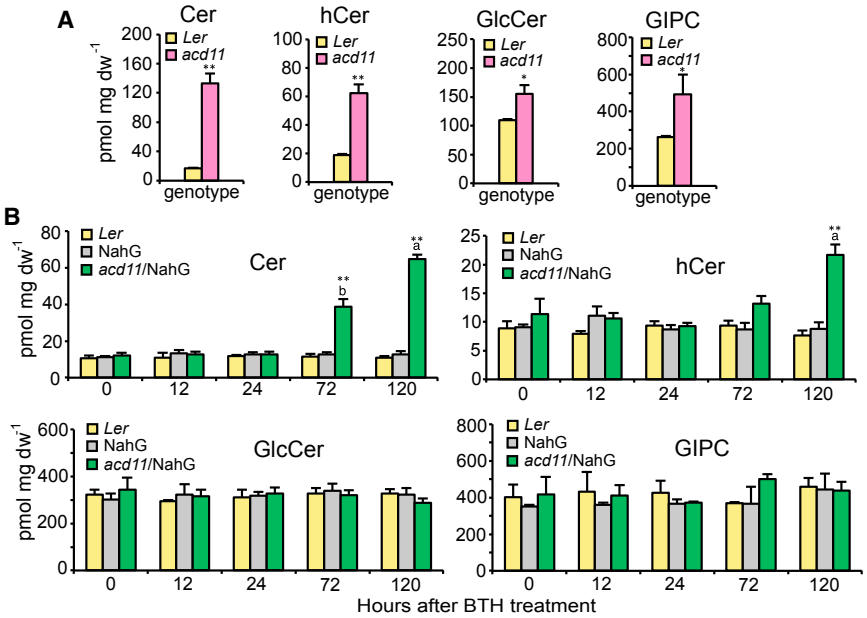

Figure 6. Constitutive and Inducible Alterations in Sphingolipid Content of *acd11* Mutants Grown at Normal Temperature

(A) Sphingolipids in leaves of dying *acd11-1* plants compared to the *Ler* WT control. Data are shown as four sphingolipid classes including phyto and nonphyto species: Cer, hydroxyceramides (hCer), GlcCer, and GIPCs. Data represent the mean ± SD (n = 3), and significant differences from the control are indicated by asterisks (**p < 0.01 and *p < 0.05) on the basis of a Student's t test. dw, dry weight.

(B) Sphingolipid contents in leaves of *acd11-1*/NahG plants 0, 12, 24, 72, and 120 hr after BTH treatment in comparison with Ler NahG and WT controls. Plants were grown for 5 weeks prior to BTH treatment. Sphingolipid contents are shown as in (A). Data represent the mean ± SE (n = 3), and letters indicate statistically different groups using one-way ANOVA with groupings by Tukey's HSD with a 95% confidence interval. **p < 0.01.

See also Figure S6.

bond with the Cer moiety amide nitrogen and oxygen ensures a highly conserved and oriented entry of the sphingolipid hydrocarbon chains into the hydrophobic pocket regardless of lipid headgroup composition. The X-ray data rectify earlier 3D homology modeling involving identification of key residues of the ACD11 lipid headgroup recognition center and location of the C terminus, i.e., Trp206 (Airenne et al., 2006).

A unique feature of the apo-ACD11 GLTP fold in comparison to other known GLTP folds including CPTP is the presence of π helix, i.e., π bulge, in helix α2 near the entrance portal of the lipid binding cleft (Figures 1G and 1J). π bulges exist in only 15% of known proteins but often at locations that enhance/regulate function (Cartailler and Luecke, 2004; Cooley et al., 2010). The π bulge in apo-ACD11 brings Asp60 and His143 sufficiently close (2.9 Å) to form a salt bridge (Figure 1G), thus providing a potential regulatory mechanism for the ACD11 GLTP fold. In other GLTP folds, a water molecule often bridges the Asp and His residues (Figure 1H). In apo-ACD11, the Asp60-His143 salt bridge created by the π bulge appears to tightly seal the entry portal region of the hydrophobic pocket (Figure 1G). In D60A-ACD11, the π bulge persists after binding 2:0-C1P, but not 12:0-C1P, suggesting that salt bridge disruption between Asp60 and His143 by itself is insufficient to induce the π helix-to-α helix conformational change needed for the ACD11/C1P complex to become "transfer viable." In addition, the C1P acyl chain needs to be longer than only two carbons. This conclusion is supported by the structure of WT-ACD11 complexed with lysoSM, which has no acyl chain but displays a bound conformation resembling that of 2:0-C1P in D60A-ACD11 (Figures 5 and S2C). LysoSM is tethered to the surface via its amine group interacting with Asp60, whereas a sulfate anion occupies the lipid headgroup (phosphate) binding pocket lending credence to the authenticity of the lysoSM binding site. Analogous behavior is observed in human GLTP/hexyl glucoside crystal complexes where the sugar headgroup occupies the glycolipid recognition center despite weak binding affinity and no measurable transfer (Malinina et al., 2006; Zhai et al., 2009). In the ACD11/lysoSM complex, occupation of the phosphate headgroup recognition center by the sulfate anion and the bulky, zwitterionic nature of the phosphocholine lipid headgroup are likely contributors to its minimal interaction and outward projection from the protein (Figure S2A). Similar conformation and surface localization are observed for the 2:0-C1P sphingosine chain in complex with D60A-ACD11 (Figure S2). Thus, despite seemingly adequate positioning on the ACD11 surface, π bulge persistence renders the lipid binding interaction insufficient to drive robust transfer.

For ACD11 to become fully "transfer viable," uptake of the sphingolipid acyl chain into the hydrophobic pocket and repositioning of specific residues appear to be required. At the molecular level, π bulge formation at Asp60 results in the Phe56 nonpolar phenyl ring projecting into the hydrophobic pocket to function as a "portal gate" that swings open during lipid acyl chain uptake (Figure 4E). Phe54 orients into the hydrophobic pocket providing conformational stability to apo-ACD11 in the absence of a lipid acyl chain. When C1P contains a sufficiently long acyl chain (e.g., 12:0-C1P), the acyl chain enters deep into the hydrophobic pocket, as shown for D60N-ACD11 and D60A-ACD11. A "peristaltic-like shift" of Ala57 to occupy the position of Phe56 as well as Phe54 being pushed outward accompanies transformation from π bulge to α helix, enabling hydrophobic pocket formation/expansion sufficient to accommodate either one or both hydrocarbon chains of Cer (Figures 4D and 4E). The key role played by Phe56 of helix α2 in functioning as a "portal gate" represents a fundamental difference between the ACD11 GLTP fold and human GLTP fold, which uses an "oppositely located" Phe (Phe148 of helix α6) as the "portal gate" that swings open during hydrocarbon chain insertion (Malinina et al., 2004; Samygina et al., 2011). The global folding topology of ACD11 and conformational adaptability of its flexible, single-cavity, hydrophobic pocket contrast with Cer

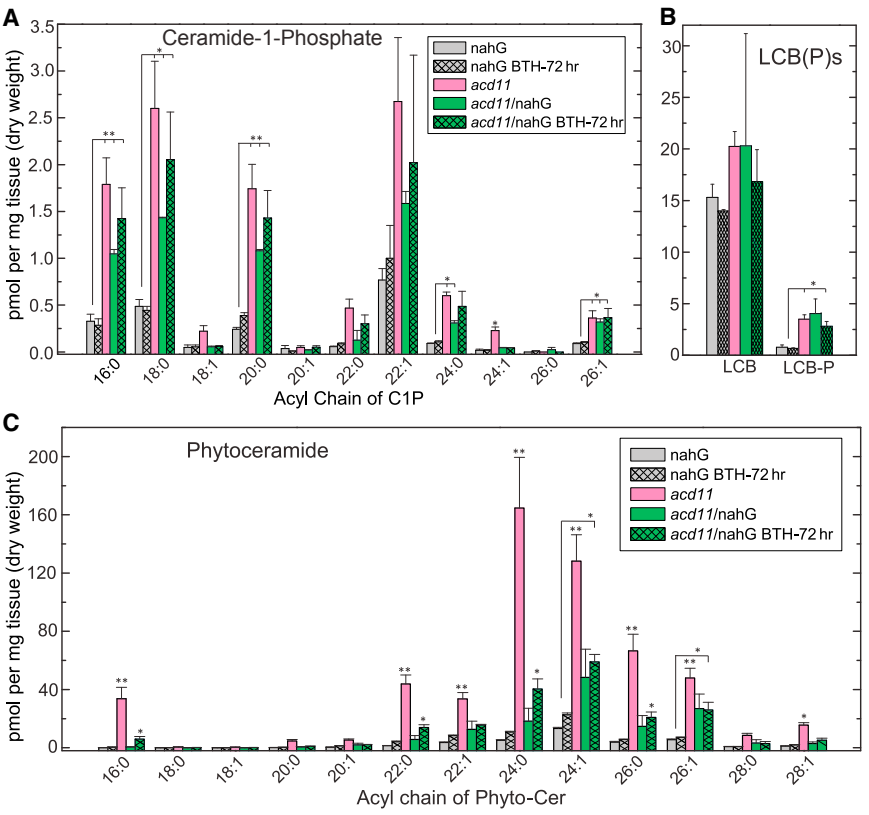

Figure 7. Constitutive and Inducible Alterations in Sphingolipid Content of *acd11* Mutants in Response to Cold-Temperature Treatment

(A–C) Sphingolipid contents of *acd11*, *acd11-1*/NahG, and control plants 72 hr after treatment with BTH. Plants were grown for 5 weeks and subjected to cold (4°C) for 4 hr prior to BTH treatment. (A) C1P. (B) LCB(P). (C) Phyto-Cer. Data represent the mean ± SE (n = 3), and significant differences from controls are indicated by asterisks (**p < 0.01 and *p < 0.05) on the basis of a Student's t test.

transfer protein, which uses an α/β fold built around an incomplete U-shaped β barrel to bind Cer via a START domain lipid cavity (Kudo et al., 2008) (see the Supplemental Discussion).

ACD11 Modulates *Arabidopsis* PCD by Intermediary Regulation of Sphingolipid Levels

The HR in plants generates localized cell death to minimize the spread of pathogens. HR-like PCD is also exhibited by the recessive *acd11-1* mutant. Despite the known ties between ACD11 and HR-like PCD (Brodersen et al., 2002), determination of the molecular structure and lipid specificity of ACD11 remained unclear until now. Establishment of ACD11 architecture as a C1P-selective GLTP fold capable of binding/transferring either C1P or phyto-C1P at similar rates provides insights into how this GLTP superfamily member impacts PCD-related processes regulated by key sphingolipid metabolites. Although fungal GLTP (HET-C2) and human FAPP2 (C-terminal GLTP-like domain) have both been implicated in PCD-related processes (Fedorova et al., 2005; Paoletti and Clavé, 2007; Tritz et al., 2009), no sphingolipid analyses were performed upon in vivo depletion of these glycosylceramide-selective GLTP folds.

Compared to mammals, plant membranes show fundamental differences in sphingolipid content including large contributions by GlcCer, GIPC, and modified sphingoid chains (e.g., phyto-derivatives) as well as a lack of SM and gangliosides (Markham et al., 2006, 2013; Pata et al., 2010). Adjustment to major lipid content during cold acclimation is well established in plants. Recent studies also show rapid elevations of low-level LCB(P)s and C1P (Cantrel et al., 2011). The established signaling functions of such lipids make them leading candidates as early signals during cold acclimation. Because LCB(P) and C1P content is low under both normal and cold-stressed growth conditions, initial detection was accomplished by radiolabeling (Cantrel et al., 2011). Determination of LCB(P) and C1P derivative mass levels has been challenging, a situation exacerbated by a dearth of authentic standards (Markham and Jaworski, 2007). This has been especially true for C1P derivatives, which had not been mass quantified in plants until the present study.

Our finding that *acd11* deficiency not only alters C1P levels but also acutely elevates phyto-Cer levels (and LCBP to a lesser extent) establishes a functional link between *acd11* expression and sphingolipid metabolic regulation in plants where the dynamic balance between Cer and C1P appears to be critical for regulating PCD (Chen et al., 2009; Liang et al., 2003; Pata et al., 2010; Reape and McCabe, 2008). Although elevated C1P levels induced by *acd11* disruption in *Arabidopsis* also are observed upon RNAi-induced depletion of the ACD11 ortholog CPTP in human cells, it is noteworthy that the dramatic elevations in phyto-Cer levels in *acd11* mutants are not duplicated in the Cer levels of CPTP-depleted human cells (Simanshu et al., 2013). This suggests some differing aspects of ACD11 involvement in the regulation of sphingolipid metabolism in plants. Elucidating the mechanistic details and associated kinetics of this involvement will first require detailed analyses of plant sphingolipid metabolic pathways, related regulatory signaling pathways, and changes triggered during cold acclimation.

What is known is that the *acd5* mutant lacks CerK activity, accumulates Cers, and exhibits PCD (Liang et al., 2003). ACD11 may act in concert with ACD5 (CerK) to maintain the balance of Cer and C1P levels, thus controlling HR-associated PCD. In this context, the loss of IPC synthase activity (*erh1* mutant) also results in total Cer accumulation, and both *erh1* and *acd5* exhibit enhanced HR-associated cell death triggered by the RPW8 resistance protein (Wang et al., 2008). However, Cer accumulation and cell death in *acd11*, *acd5*, and *erh1* are dependent on the phytohormone, SA. This suggests that

perturbations in sphingolipid metabolism, such as occur in *acd11*, may regulate SA levels or signaling during R gene-mediated HR. Plant R proteins confer recognition of pathogen avirulence proteins and trigger effective innate immune responses (e.g., HR). A genetic screen for suppressors of *acd11* cell death (*laz* mutants) identified the *R* gene *LAZ5*. Thus, the absence of ACD11 in *acd11* leads to inappropriate HR activation by LAZ5 (Palma et al., 2010). Because sphingolipids are important in both microbial pathogenesis and host defense (Heung et al., 2006), LAZ5 may "guard" ACD11 function(s) in certain sphingolipid metabolic pathways targeted by pathogen effectors. Also, transgenic expression of human WT-GLTP and D48V-GLTP (Petersen et al., 2008) suppresses *acd11* cell death, raising the possibility that the C1P binding/transfer activity of ACD11 is partially dispensable for PCD suppression. This could implicate LAZ5 as a response amplifier that triggers the HR when the local distribution and balance between phyto-Cer and C1P are disturbed, thereby intensifying the response through SA accumulation. Pathogen effector-induced modification or loss of function of ACD11 could interfere with normal sphingolipid distribution and trigger a defense response strong enough to deter microbial colonization. Because sphingolipid bases are upregulated early during an infection or HR, it is probable that sphingolipids are signaling mediators, and not the de facto cell death inducers via membrane perturbations (Mackey et al., 2003; Peer et al., 2010). Testing this hypothesis will require research to clarify the interplay between cellular sphingolipid metabolism and basal immunity in plants.

It is also possible that loss of ACD11 as a selective carrier blocks C1P exit from the Golgi resulting in organelle stress, as occurs in human cells depleted of the ACD11 ortholog, CPTP (Simanshu et al., 2013), and leading to local accumulation of Cer that alters membrane component organization. Because ACD11 may be indirectly guarded (Palma et al., 2010), triggering of HR cell death may not rely directly on the absence of ACD11 in the *acd11* mutant. In mammals, nonmicrobial "danger signals" instigate obesity-induced inflammation via NLRP3, which senses increasing Cer and induces apoptosis (Vandanmagsar et al., 2011), providing a potential clue as to how the HR might be induced in *acd11* by LAZ5 via detection of the accumulation of specific sphingolipid species. Future localization studies on ACD11 and LAZ5 to evaluate possible corestriction in specific organelles could provide more insights.

EXPERIMENTAL PROCEDURES

Cloning, Expression, and Purification

acd11-1 open reading frame (ORF; GenBank accession number NCBI NP_181016.1) expression in BL21(DE3) pLysS cells using pET-SUMO vector (Invitrogen) enabled Ni^{2+}-NTA affinity chromatography purification of ACD11 N-terminally tagged with His_6-SUMO (see Supplemental Experimental Procedures). Pure proteins were either used for crystallization immediately or flash frozen in liquid N_2 and stored at −80°C. ACD11 mutants were generated by PCR-based overlap extension and confirmed by DNA sequencing. Expression/purification was the same as for WT-ACD11.

Crystallization

A Mosquito crystallization robot (Molecular Dimensions) was used for initial cocrystallization screening of WT-ACD11 and the D60N and D60A mutants with lysoSM and C1P species (see the Supplemental Experimental Procedures). Positive hits were optimized using the hanging drop vapor diffusion method by varying pH and concentration of individual components (Table S3). For data collection, crystals were flash frozen (100 K) in crystallization condition containing 25% (v/v) ethylene glycol. Diffraction data sets were collected on 24-ID-C and 24-ID-E beamlines at the Advanced Photon Source and X29A beamline at National Synchrotron Light Source. Collected data sets were integrated and scaled using the HKL2000 suite (Otwinowski and Minor, 1997). All crystals have different packing interactions leading to different unit cell dimensions and space groups (Table S1).

Structure Determination and Refinement

Ab initio phasing was obtained by soaking apo-ACD11 crystals in 1 mM ethyl mercuric phosphate for 24 hr and collecting data (2.45 Å resolution) using a Rigaku RU-H3R X-ray generator equipped with a RAXIS-HTC detector (Table S2). ACD11 structure was determined by the SIRAS method using Hg isomorphous as well as anomalous scattering data, with the 8 Hg sites located and refined for phasing using SHARP (Vonrhein et al., 2007). apo-ACD11 crystals belonged to space group $P2_12_12_1$ and contained four protein molecules per asymmetric unit. The structures of ACD11-sphingolipid complexes were solved by molecular replacement (MOLREP program) using apo-ACD11 (Hg derivative) structure as the search model (Vagin and Teplyakov, 1997) (see the Supplemental Experimental Procedures).

ACD11 Intermembrane Lipid Transfer Activity

Förster resonance energy transfer provided kinetic insights into lipid transfer by ACD11. Donor POPC vesicles, containing 1 mol% AV-lipid acylated with (11*E*)-12-(9-anthryl)-11-dodecenoate and 1.5 mol% 1-acyl-2-[9-(3-perylenoyl)-nonanoyl]-3-*sn*-glycero-3-phosphocholine (Per-PC) were prepared by rapid ethanol injection (Mattjus et al., 1999). In competition assays, donor vesicles contained 1 mol% AV-C1P (Boldyrev et al., 2013) as well as 0.5, 1.0, or 2.0 mol% competitor lipids (Samygina et al., 2011). Both fluorescent lipids were present initially only in donor vesicles where minimal AV emission occurs upon excitation (370 nm) because of energy transfer to Per-PC. ACD11 addition results in an exponential increase in AV emission intensity as the protein transports AV-C1P from donor vesicles (creating separation from the "nontransferable" Per-PC) and delivers to the 10-fold excess POPC acceptor vesicles. The time-dependent increase in AV emission at 425 nm, relative to baseline fluorescence in the absence of ACD11, yields the AV-C1P transfer kinetics (see the Supplemental Experimental Procedures).

Plant Material and Sphingolipid Analyses

acd11-1, *acd11/NahG*, and *NahG* plants in *Ler* background have been described by Brodersen et al. (2005). For sphingolipid analyses, plants were grown in soil under short days (8 hr light/16 hr dark) in chambers at 150 mE/m^2s, 21°C, and 70% relative humidity. *Ler* WT and *acd11-1* mutants were grown untreated for 4 weeks before sampling. *acd11-1/NahG* together with *NahG* and *Ler* plants were grown for 5 weeks prior to spraying with the SA analog BTH (100 μM) and sampling after 0, 12, 24, 72, and 120 hr. Leaf material was harvested from three biological replicates for each genotype and time point. Sphingolipid analysis was performed by mass spectrometry (Bielawski et al., 2009; Markham and Jaworski, 2007). Free and total LCBs were analyzed by HPLC after fluorescent derivatization (Bach et al., 2008).

ACCESSION NUMBERS

The atomic coordinates and structure factors for the crystal structures of *Arabidopsis* WT-ACD11 and mutants in complex with various lipids were deposited in the Protein Data Bank under accession numbers 4NT1 (apo-ACD11), 4NT2 (ACD11/lysoSM), 4NTI (D60N-ACD11/12:0-C1P), 4NTG (D60A-ACD11/12:0-C1P), and 4NTO (D60A-ACD11/2:0-C1P).

SUPPLEMENTAL INFORMATION

Supplemental Information includes Supplemental Discussion, Supplemental Experimental Procedures, seven figures, and three tables and can be found with this article online at http://dx.doi.org/10.1016/j.celrep.2013.12.023.

AUTHOR CONTRIBUTIONS

D.K.S. performed all structural analyses and provided definitive evidence for C1P binding by ACD11, generated all ACD11 point mutants, and wrote the text. X.Z. first showed C1P transfer by WT-ACD11, completed all transfer analyses of WT-ACD11 and ACD11 point mutants, and wrote the text. D.M. and D.H. prepared *Arabidopsis* mutants for sphingolipidomic analyses and wrote the text. J.E.M. performed time-based sphingolipidomic analyses on *Arabidopsis* mutants and wrote the text. J.B. and A.B. completed sphingolipidomic analyses on cold-treated *Arabidopsis* mutants. J.G.M. synthesized fluorescent lipids. L.M. contributed to structural data interpretation. J.W.M. directed the setup of *Arabidopsis* mutant analyses and finalized the write-up. D.J.P. directed ACD11 structural analyses and finalized the write-up. R.E.B. directed functional and structural analyses, finalized the write-up, and coordinated and integrated all section write-ups.

ACKNOWLEDGMENTS

This research was supported by NIH/NIGMS GM45928 (to R.E.B.), NIH/NCI CA121493 (to D.J.P. and R.E.B.), Danish Strategic Research Council 09-067148 (to J.W.M.), NSF/MCB 0843312 (to J.E.M.), NIH/NCRR C06 RR018823 (to J.B. and A.B.), Spanish Ministerio de Ciencia e Innovacion BFU2010-17711 (to L.M.), Russian Foundation for Basic Research #12-04-00168 (to J.G.M.), Hormel Foundation (to R.E.B.), Abby Rockefeller Mauze Trust (to D.J.P.), and Maloris Foundation (to D.J.P.). We thank J. Peter Slotte (Åbo Akademi University) for the IPC lipid, Helen Pike (UMN-Hormel Institute) for purifying protein used for transfer activity analyses, and the staff of X-29 beamline at the National Synchrotron Light Source and ID-24-C/E beamlines at the Advanced Photon Source for help. The Lipidomics Shared Resource MUSC is partially supported by P30 CA138313, HCC, and P20 RR017677 SC COBRE in Lipidomics and Pathobiology.

Received: June 19, 2013
Revised: October 21, 2013
Accepted: December 12, 2013
Published: January 9, 2014

REFERENCES

Airenne, T.T., Kidron, H., Nymalm, Y., Nylund, M., West, G., Mattjus, P., and Salminen, T.A. (2006). Structural evidence for adaptive ligand binding of glycolipid transfer protein. J. Mol. Biol. *355*, 224–236.

Bach, L., Michaelson, L.V., Haslam, R., Bellec, Y., Gissot, L., Marion, J., Da Costa, M., Boutin, J.-P., Miquel, M., Tellier, F., et al. (2008). The very-long-chain hydroxy fatty acyl-CoA dehydratase PASTICCINO2 is essential and limiting for plant development. Proc. Natl. Acad. Sci. USA *105*, 14727–14731.

Berkey, R., Bendigeri, D., and Xiao, S. (2012). Sphingolipids and plant defense/disease: the "death" connection and beyond. Front Plant Sci *3*, 68.

Bielawski, J., Pierce, J.S., Snider, J., Rembiesa, B., Szulc, Z.M., and Bielawska, A. (2009). Comprehensive quantitative analysis of bioactive sphingolipids by high-performance liquid chromatography-tandem mass spectrometry. Methods Mol. Biol. *579*, 443–467.

Boldyrev, I.A., Brown, R.E., and Molotkovsky, J.G. (2013). An expedient synthesis of fluorescent labeled ceramide-1-phosphate analogues. Russ. J. Bioorganic Chem. *39*, 539–542.

Brodersen, P., Petersen, M., Pike, H.M., Olszak, B., Skov, S., Odum, N., Jørgensen, L.B., Brown, R.E., and Mundy, J. (2002). Knockout of *Arabidopsis* accelerated-cell-death11 encoding a sphingosine transfer protein causes activation of programmed cell death and defense. Genes Dev. *16*, 490–502.

Brodersen, P., Malinovsky, F.G., Hématy, K., Newman, M.A., and Mundy, J. (2005). The role of salicylic acid in the induction of cell death in *Arabidopsis* acd11. Plant Physiol. *138*, 1037–1045.

Brown, R.E., and Mattjus, P. (2007). Glycolipid transfer proteins. Biochim. Biophys. Acta *1771*, 746–760.

Cantrel, C., Vazquez, T., Puyaubert, J., Rezé, N., Lesch, M., Kaiser, W.M., Dutilleul, C., Guillas, I., Zachowski, A., and Baudouin, E. (2011). Nitric oxide participates in cold-responsive phosphosphingolipid formation and gene expression in *Arabidopsis thaliana*. New Phytol. *189*, 415–427.

Cartailler, J.P., and Luecke, H. (2004). Structural and functional characterization of pi bulges and other short intrahelical deformations. Structure *12*, 133–144.

Chen, M., Cahoon, E.B., Saucedo-García, M., Plasencia, J., and Gavilanes-Ruíz, M. (2009). Plant sphingolipids: structure, synthesis, function. In Lipids in Photosynthesis: Essential and Regulatory Functions, H. Wada and N. Murata, eds. (New York: Springer Science), pp. 77–115.

Cooley, R.B., Arp, D.J., and Karplus, P.A. (2010). Evolutionary origin of a secondary structure: π-helices as cryptic but widespread insertional variations of α-helices that enhance protein functionality. J. Mol. Biol. *404*, 232–246.

Fedorova, N.D., Badger, J.H., Robson, G.D., Wortman, J.R., and Nierman, W.C. (2005). Comparative analysis of programmed cell death pathways in filamentous fungi. BMC Genomics *6*, 177.

Fyrst, H., and Saba, J.D. (2010). An update on sphingosine-1-phosphate and other sphingolipid mediators. Nat. Chem. Biol. *6*, 489–497.

Hannun, Y.A., and Obeid, L.M. (2008). Principles of bioactive lipid signalling: lessons from sphingolipids. Nat. Rev. Mol. Cell Biol. *9*, 139–150.

Heung, L.J., Luberto, C., and Del Poeta, M. (2006). Role of sphingolipids in microbial pathogenesis. Infect. Immun. *74*, 28–39.

Hwang, O., Kim, G., Jang, Y.J., Kim, S.W., Choi, G., Choi, H.J., Jeon, S.Y., Lee, D.G., and Lee, J.D. (2001). Synthetic phytoceramides induce apoptosis with higher potency than ceramides. Mol. Pharmacol. *59*, 1249–1255.

Kamlekar, R.K., Simanshu, D.K., Gao, Y.G., Kenoth, R., Pike, H.M., Prendergast, F.G., Malinina, L., Molotkovsky, J.G., Venyaminov, S.Y., Patel, D.J., and Brown, R.E. (2013). The glycolipid transfer protein (GLTP) domain of phosphoinositol 4-phosphate adaptor protein-2 (FAPP2): structure drives preference for simple neutral glycosphingolipids. Biochim. Biophys. Acta *1831*, 417–427.

Kenoth, R., Simanshu, D.K., Kamlekar, R.K., Pike, H.M., Molotkovsky, J.G., Benson, L.M., Bergen, H.R., 3rd, Prendergast, F.G., Malinina, L., Venyaminov, S.Y., et al. (2010). Structural determination and tryptophan fluorescence of heterokaryon incompatibility C2 protein (HET-C2), a fungal glycolipid transfer protein (GLTP), provide novel insights into glycolipid specificity and membrane interaction by the GLTP fold. J. Biol. Chem. *285*, 13066–13078.

Kenoth, R., Kamlekar, R.K., Simanshu, D.K., Gao, Y., Malinina, L., Prendergast, F.G., Molotkovsky, J.G., Patel, D.J., Venyaminov, S.Y., and Brown, R.E. (2011). Conformational folding and stability of the HET-C2 glycolipid transfer protein fold: does a molten globule-like state regulate activity? Biochemistry *50*, 5163–5171.

Kudo, N., Kumagai, K., Tomishige, N., Yamaji, T., Wakatsuki, S., Nishijima, M., Hanada, K., and Kato, R. (2008). Structural basis for specific lipid recognition by CERT responsible for nonvesicular trafficking of ceramide. Proc. Natl. Acad. Sci. USA *105*, 488–493.

Lam, E. (2004). Controlled cell death, plant survival and development. Nat. Rev. Mol. Cell Biol. *5*, 305–315.

Liang, H., Yao, N., Song, J.T., Luo, S., Lu, H., and Greenberg, J.T. (2003). Ceramides modulate programmed cell death in plants. Genes Dev. *17*, 2636–2641.

Mackey, D., Belkhadir, Y., Alonso, J.M., Ecker, J.R., and Dangl, J.L. (2003). *Arabidopsis* RIN4 is a target of the type III virulence effector AvrRpt2 and modulates RPS2-mediated resistance. Cell *112*, 379–389.

Malinina, L., Malakhova, M.L., Teplov, A., Brown, R.E., and Patel, D.J. (2004). Structural basis for glycosphingolipid transfer specificity. Nature *430*, 1048–1053.

Malinina, L., Malakhova, M.L., Kanack, A.T., Lu, M., Abagyan, R., Brown, R.E., and Patel, D.J. (2006). The liganding of glycolipid transfer protein is controlled by glycolipid acyl structure. PLoS Biol. *4*, e362.

Markham, J.E., and Jaworski, J.G. (2007). Rapid measurement of sphingolipids from *Arabidopsis thaliana* by reversed-phase high-performance liquid

chromatography coupled to electrospray ionization tandem mass spectrometry. Rapid Commun. Mass Spectrom. *21*, 1304–1314.

Markham, J.E., Li, J., Cahoon, E.B., and Jaworski, J.G. (2006). Separation and identification of major plant sphingolipid classes from leaves. J. Biol. Chem. *281*, 22684–22694.

Markham, J.E., Lynch, D.V., Napier, J.A., Dunn, T.M., and Cahoon, E.B. (2013). Plant sphingolipids: function follows form. Curr. Opin. Plant Biol. *16*, 350–357.

Mattjus, P., Molotkovsky, J.G., Smaby, J.M., and Brown, R.E. (1999). A fluorescence resonance energy transfer approach for monitoring protein-mediated glycolipid transfer between vesicle membranes. Anal. Biochem. *268*, 297–304.

Michaelson, L.V., and Napier, J.A. (2010). Sphingolipid signaling in plants. In Lipid Signaling in Plants, Plant Cell Monographs, T. Munnik, ed. (Heidelberg: Springer-Verlag), pp. 307–321.

Otwinowski, Z., and Minor, W. (1997). Processing of X-ray diffraction data collected in oscillation mode. Methods Enzymol. *276*, 307–326.

Palma, K., Thorgrimsen, S., Malinovsky, F.G., Fiil, B.K., Nielsen, H.B., Brodersen, P., Hofius, D., Petersen, M., and Mundy, J. (2010). Autoimmunity in *Arabidopsis* acd11 is mediated by epigenetic regulation of an immune receptor. PLoS Pathog. *6*, e1001137.

Paoletti, M., and Clavé, C. (2007). The fungus-specific HET domain mediates programmed cell death in Podospora anserina. Eukaryot. Cell *6*, 2001–2008.

Pata, M.O., Hannun, Y.A., and Ng, C.K. (2010). Plant sphingolipids: decoding the enigma of the Sphinx. New Phytol. *185*, 611–630.

Peer, M., Stegmann, M., Mueller, M.J., and Waller, F. (2010). *Pseudomonas syringae* infection triggers de novo synthesis of phytosphingosine from sphinganine in *Arabidopsis thaliana*. FEBS Lett. *584*, 4053–4056.

Petersen, N.H., McKinney, L.V., Pike, H., Hofius, D., Zakaria, A., Brodersen, P., Petersen, M., Brown, R.E., and Mundy, J. (2008). Human GLTP and mutant forms of ACD11 suppress cell death in the *Arabidopsis* acd11 mutant. FEBS J. *275*, 4378–4388.

Reape, T.J., and McCabe, P.F. (2008). Apoptotic-like programmed cell death in plants. New Phytol. *180*, 13–26.

Samygina, V.R., Popov, A.N., Cabo-Bilbao, A., Ochoa-Lizarralde, B., Goni-de-Cerio, F., Zhai, X., Molotkovsky, J.G., Patel, D.J., Brown, R.E., and Malinina, L. (2011). Enhanced selectivity for sulfatide by engineered human glycolipid transfer protein. Structure *19*, 1644–1654.

Samygina, V.R., Ochoa-Lizarralde, B., Popov, A.N., Cabo-Bilbao, A., Goni-de-Cerio, F., Molotkovsky, J.G., Patel, D.J., Brown, R.E., and Malinina, L. (2013). Structural insights into lipid-dependent reversible dimerization of human GLTP. Acta Crystallogr. D Biol. Crystallogr. *69*, 603–616.

Simanshu, D.K., Kamlekar, R.K., Wijesinghe, D.S., Zou, X., Zhai, X., Mishra, S.K., Molotkovsky, J.G., Malinina, L., Hinchcliffe, E.H., Chalfant, C.E., et al. (2013). Non-vesicular trafficking by a ceramide-1-phosphate transfer protein regulates eicosanoids. Nature *500*, 463–467.

Tritz, R., Hickey, M.J., Lin, A.H., Hadwiger, P., Sah, D.W., Neuwelt, E.A., Mueller, B.M., and Kruse, C.A. (2009). FAPP2 gene downregulation increases tumor cell sensitivity to Fas-induced apoptosis. Biochem. Biophys. Res. Commun. *383*, 167–171.

Vagin, A., and Teplyakov, A. (1997). MOLREP: an automated program for molecular replacement. J. Appl. Crystallogr. *30*, 1022–1025.

Vandanmagsar, B., Youm, Y.H., Ravussin, A., Galgani, J.E., Stadler, K., Mynatt, R.L., Ravussin, E., Stephens, J.M., and Dixit, V.D. (2011). The NLRP3 inflammasome instigates obesity-induced inflammation and insulin resistance. Nat. Med. *17*, 179–188.

Vonrhein, C., Blanc, E., Roversi, P., and Bricogne, G. (2007). Automated structure solution with autoSHARP. Methods Mol. Biol. *364*, 215–230.

Wang, W., Yang, X., Tangchaiburana, S., Ndeh, R., Markham, J.E., Tsegaye, Y., Dunn, T.M., Wang, G.L., Bellizzi, M., Parsons, J.F., et al. (2008). An inositolphosphorylceramide synthase is involved in regulation of plant programmed cell death associated with defense in *Arabidopsis*. Plant Cell *20*, 3163–3179.

West, G., Viitanen, L., Alm, C., Mattjus, P., Salminen, T.A., and Edqvist, J. (2008). Identification of a glycosphingolipid transfer protein GLTP1 in *Arabidopsis thaliana*. FEBS J. *275*, 3421–3437.

Zhai, X., Malakhova, M.L., Pike, H.M., Benson, L.M., Bergen, H.R., 3rd, Sugár, I.P., Malinina, L., Patel, D.J., and Brown, R.E. (2009). Glycolipid acquisition by human glycolipid transfer protein dramatically alters intrinsic tryptophan fluorescence: insights into glycolipid binding affinity. J. Biol. Chem. *284*, 13620–13628.